PAPER

Check for updates

A highly active and chemoselective homobimetallic ruthenium catalyst for one-pot reductive amination in water†

Gopal Deshmukh, [ID] Thakur Rochak Kumar Rana, Nikita Yadav, Gopalan Rajaraman [ID] * and Ramaswamy Murugavel [ID] *

The first ever homobimetallic catalyst which efficiently catalyzes the reductive amination (RA) reaction of carbonyl compounds in water is described herein. Two new Ru(II) compounds, homobimetallic [(*p*-cymene)$_2$(RuCl)$_2$L^1] (**Ru1**) and monometallic [(*p*-cymene)(RuCl)L^2] (**Ru2**) (where L^1 = 2,2′-((1E,1′E)-((3,3′,5,5′-tetraisopropyl-[1,1′-biphenyl]-4,4′-diyl)bis-(azaneylylidene))bis(methaneylylidene))diphenoxide) and L^2 = (2,6-(((diisopropylphenyl)-imino)methyl)phenoxide) incorporating Schiff-base ligands have been synthesized and characterized by various spectroscopic and analytical techniques. Their molecular structures have been deduced by X-ray diffraction measurements. Both complexes, which are water/air stable at room temperature as well as at high temperature, were employed as catalysts for RA in aqueous media using formate buffer as the hydrogen source. Complex **Ru1**, in the presence of formic acid/formate buffer as the hydrogen source, catalyzes one-pot RA production of secondary amines in ~99% yield with just 0.05 mol% of the catalyst exhibiting a turnover number (TON) of 1920 and a turnover frequency (TOF) of 480 h^{-1}. When the catalyst loading was further reduced to 0.0001 mol%, the highest reported TON and TOF for any RA reactions were observed (4.3×10^4 and 107×10^3 h^{-1}, respectively), albeit with reduced selectivity. A comparative study between **Ru1** and **Ru2** reveals that complex **Ru1** is more chemo-selective for the formation of a secondary amine, attributable to a cooperative effect. This cooperative effect is further substantiated through extensive computational methodologies involving Density Functional Theory (DFT) calculations on both bimetallic and monometallic Ru(II) complexes along a hybrid-model complex.

Introduction

Amines are one of the vital components in organic synthesis, materials science, and chemical industries like agrochemicals, pharmaceuticals, and fine chemicals.[1,2] Consequently, enormous efforts have been focused on the large-scale synthesis of amines. In particular, secondary amines have gained tremendous attention compared to primary and tertiary amines due to their applications in dyes, plastics, fragrances and pharmaceutical products such as anti-Chagas disease drugs and anti-depressant drugs.[2-6] Common approaches for the production of the former include the dehydrohalogenation reaction between amines and alkyl halides,[7] reductions of amides and imines,[8-10] RA using carbonyls,[11-16] borrowing hydrogenation

of alcohols as well as hydrogenation of nitriles.[17,18] However, uncontrolled dehydrohalogenation reactions lead to the formation of tertiary amines, and copious amounts of by-products make it unsatisfactory. The imine reduction method requires pre-synthesized imines and demands either external H$_2$ pressure or reagents like borohydrides or silanes. The instability of imines also restricts their usage.[19] Moreover, the borrowing hydrogenation method is energy intensive since it requires higher reaction temperatures (80–150 °C) in an organic solvent such as toluene, xylene or 1,4-dioxane.[18,20,21] On the other hand, the RA reactions occur at around 80 °C in polar protic solvents.[13,14] Thus, the RA method has emerged as a very promising alternative using both homogeneous and heterogeneous catalysts based on Co, Rh, Ir, Fe, Ru, Ni, and Pd.[10,22-32] Although the development of newer and more efficient RA catalysts is currently witnessing enormous activity,[33,34] there is ample scope for further improvements in all catalytic parameters, *viz.* catalyst load, overall yield, selectivity, TON, TOF, *etc.*

Hydrogen gas has been commonly employed as the hydride source in most of the earlier reported RA reactions catalysed

Department of Chemistry, Indian Institute of Technology Bombay, Powai, Mumbai 400 076, India. E-mail: rajaraman@chemiitb.ac.in, rmv@chem.iitb.ac.in
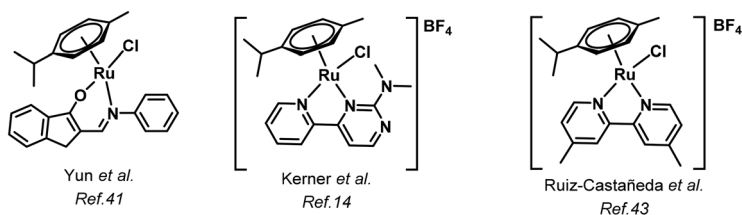
by heterogeneous (and also homogeneous) transition metal catalysts.[22,35–37] Besides, heterogeneous catalysts often lead to low chemoselectivity apart from the difficulties associated with the spectroscopic monitoring of intermediates. This demands the development of molecular catalysts for a better understanding and selectivity of the RA reaction.[22,36] However, to date there are only a few examples of selective RA catalysts in the literature which employ water as the reaction medium or do not use H_2 as a hydride source.[38–41] These examples use formic acid/formate buffer as an alternative hydride source since it is mild, selective, and less hazardous.[24,41,42] Moreover, reactions performed in organic solvents generally employ H_2,[37] while formate buffer is the preferred hydrogen source in the aqueous medium for better miscibility and homogeneity. This system also offers new reactivity and selectivity.

Collectively, high catalyst loading, harsher reaction conditions, use of organic solvents, use of hazardous H_2 as a hydrogen source, lack of chemoselectivity, low green metrics and sustainability still remain challenges for further develop-
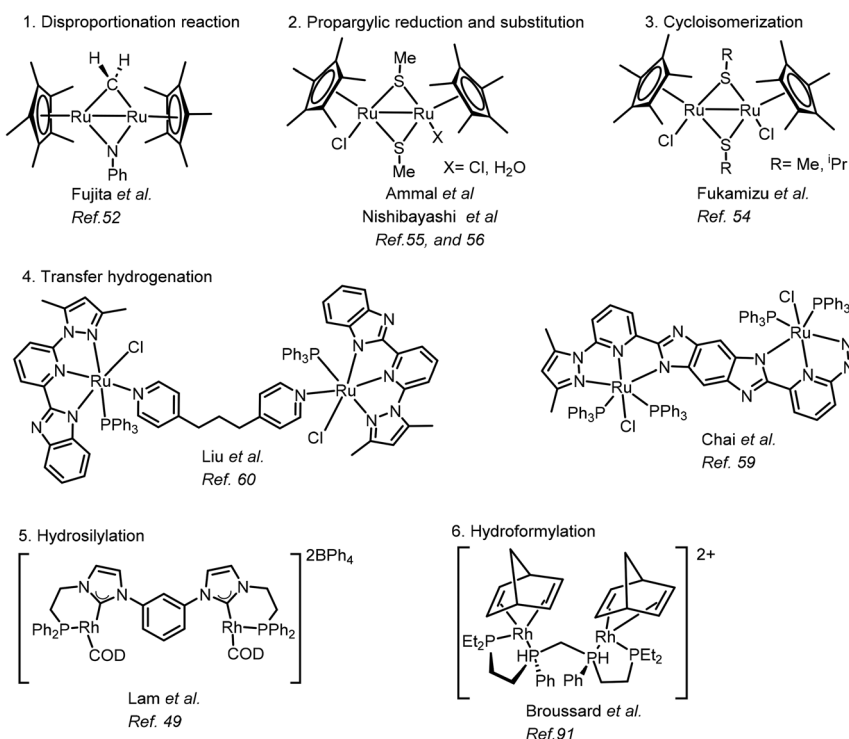
ment in this field.[14,33,41–44] One way to tackle such a complex combination of challenges would be to design bimetallic (or multimetallic) catalyst systems that can operate in the aqueous medium and utilize formate buffer as a hydride source and still exhibit high selectivity for the secondary amine production *via* RA.

Bimetallic catalysts can enhance the rate and selectivity of a catalyzed reaction to a significant level.[45–48] The improved efficiency of a bimetallic catalyst compared to its monometallic analog can be ascribed to cooperative interactions between the two metals and any possible electronic communication through bridging organic ligands.[49,50] Bimetallic catalysts can be of two types, *viz.* homobimetallic (same metals) and heterobimetallic (different metals). In the literature, several examples of bimetallic catalysts have been reported due to their superiority in various organic transformations (Scheme 1). These include hydroformylation,[46,48] hydroelementation of alkynes,[51] disproportionation of formic acid to methanol,[52] hydroamination,[53] cycloisomerisation,[54] and propargylic reduction and

Scheme 1 A selection of earlier reported monometallic catalysts employed for RA reactions and bimetallic catalysts for other organic transformations.

substitution reactions.[55,56] For example, Pernik and co-workers[49] have shown that a bimetallic rhodium complex is more active than a monometallic catalyst for hydrosilylation. Similarly, a dinuclear nickel catalyst that is significantly more active than its mononuclear counterpart in alkyne hydrosilylation was reported by Uyeda and co-workers.[57] Similarly, a Ni-bimetallic complex reported by Ackermann and co-workers promotes C–H alkylation of aniline with alkyl halides,[58] while bimetallic ruthenium pincer complexes described by Yu and co-workers effectively perform transfer hydrogenation of ketones using isopropanol as a hydrogen source.[51,59–61]

Despite the exceptional performance exhibited by homo- or hetero-bimetallic catalysts in various organic transformations shown in Scheme 1, the reductive amination of carbonyl compounds has never been probed by bimetallic catalysis in order to evaluate the relevance of cooperative catalysis in RA. To bridge this gap, the present work showcases for the first time the use of a homobimetallic catalyst (**Ru1**; Scheme 2) for selective and efficient RA of a variety of substrates in water, apart from providing meaningful comparisons with the catalytic performance of its mononuclear counterpart (**Ru2**). The role of two metals *versus* one has also been further probed by detailed DFT calculations.

Results and discussion

Synthesis and characterization of complexes [(*p*-cymene)$_2$(RuCl)$_2$L^1] (Ru1) and [(*p*-cymene)(RuCl)L^2] (Ru2)

Salicylaldimine ligands 2,2′-((1*E*,1′*E*)-((3,3′,5,5′-tetraisopropyl-[1,1′-biphenyl]-4,4′diyl)bis(azaneylylidene))bis(methaneylylidene))diphenol (**H$_2$L^1**) and 2,6-(((diisopropylphenyl)imino)methyl)phenol (**HL^2**) were synthesized by condensation of salicylaldehyde with 2,2′,6,6′-tetraisopropylbenzidine and 2,6-diisopropylaniline, respectively.[62–64] Complexes **Ru1** and **Ru2** were prepared in high yields by modifying a reported procedure.[65,66] Their typical synthesis involves the reactions between [Ru(*p*-cymene)(μ-Cl)Cl]$_2$ and salicylaldimine **H$_2$L^1** or **HL^2** in the presence of potassium carbonate as a base in ethanol at room temperature (Scheme 3). Crude products pre-
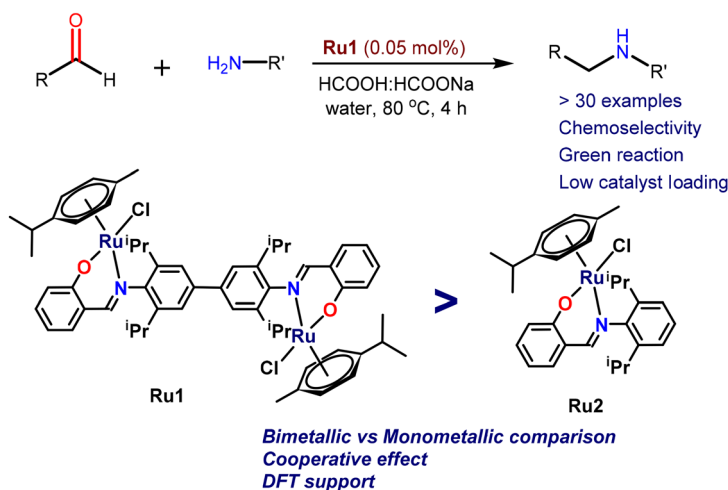
Scheme 2 Bimetallic and monometallic catalysts employed in the present study for RA of aldehydes.
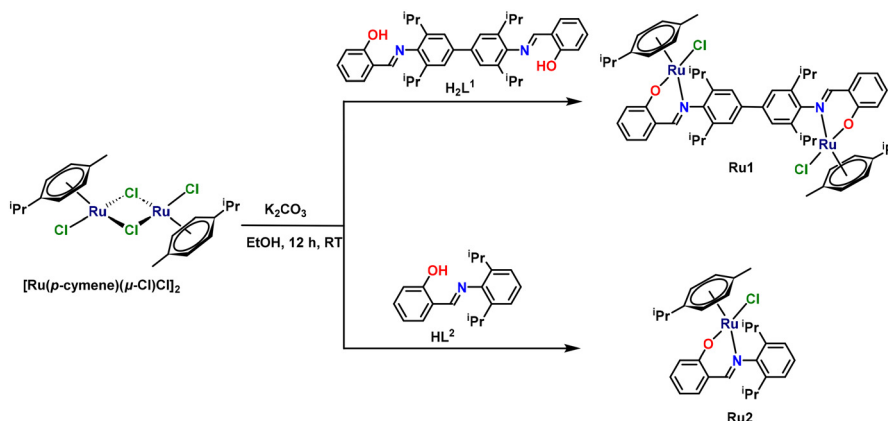
Scheme 3 Synthesis of complexes **Ru1** and **Ru2**.

cipitate out as dark red solids which were recrystallized from the dichloromethane : ethanol (4 : 1 v/v) mixture. **Ru1** and **Ru2** were further characterized by spectroscopic and analytical techniques.

In the FT-IR spectra of **Ru1** and **Ru2**, the absence of absorption bands around 3300 cm^{-1} reveals the complete deprotonation of the OH groups. The strong band at 1610 cm^{-1} (which is shifted from 1629 cm^{-1} for the free ligand) confirms the formation of the Ru–N═C bond and thus the transfer of the electron density from Ru(II) to the ligand (Fig. S1 and S9†). Formation of the desired product in both cases is confirmed by ESI-MS, which shows intense peaks at m/z 1065.3069 and 526.1818 corresponding to the [M − Cl]$^{+}$ ion for **Ru1** and **Ru2**, respectively (Fig. S2 and S6†). Additional evidence was gathered from NMR spectroscopy studies. In the ^{1}H NMR spectra of **Ru1** and **Ru2**, six doublets for the methyl group (δ 1.48–1.14 ppm) and five doublets (δ 1.48–1.03 ppm) for the isopropyl moieties have been observed, respectively (Fig. S3 and S7†). Two septets (δ 3.30, 2.85 ppm) for the isopropyl groups of p-cymene and the benzidine moiety have been observed. Four doublets in the region δ 5.48–4.37 ppm (upfield shift from free cymene confirms Ru–cymene bond formation) represent the phenyl protons of cymene. The ^{13}C NMR (Figure S4 and S8) and remaining ^{1}H NMR signals indicate the formation of the desired product.

The UV-vis spectra of the ligands **H$_2$L^1** and **HL^2** and complexes **Ru1** and **Ru2** have been recorded in the wavelength range of 800–200 nm in dichloromethane (DCM) at room temperature to investigate the electronic structures and the coordination mode of the metal centre (Fig. S10–S12†). Two well-separated absorption bands observed around 272–250 and 350–335 nm in the UV–vis spectra of the ligands **H$_2$L^1** and **HL^2** are ascribed to the intra-ligand transition originating from the $\pi \rightarrow \pi^*$ and $n \rightarrow \pi^*$ transitions of the phenyl rings of ligands.

Time-dependent DFT (TD-DFT) calculations reveal two intense bands at 293 (exp. 275) and 371 (exp. 340) nm for **Ru1**,

indicating strong charge transfer corresponding to the $\pi \rightarrow \pi^*$ inter-ligand transition. We also observed two bands at 448 nm ($d_{yz} \rightarrow d_{x_2-y_2}$) and 485 nm ($d_{xz} \rightarrow d_{z_2}$) for metal-to-metal charge transfer, in addition to a band at 537 nm ($d_{yz} \rightarrow \pi^*$) for metal-to-ligand charge transfer. These findings are in good agreement with experiments, validating our computational approach. The band at 371 nm can be observed only when spectra are recorded at a high concentration, which is shown in Fig. 1.

Molecular structure of Ru1 and Ru2

Single crystals of homobimetallic **Ru1** and monometallic **Ru2** complexes suitable for X-ray diffraction analysis were obtained by recrystallization of the red powder obtained from the dichloromethane : ethanol solvent mixture under ambient conditions by slow evaporation of the solvent. In both the complexes, each of the Ru centers adopts a distorted octahedral geometry and is coordinated to the nitrogen atom of imine, an oxygen atom of the phenolic –OH group of the Schiff base, the chloride ion, and η^6-cymene. The molecular structures of **Ru1** and **Ru2** are shown in Fig. 2. The Ru–N bond lengths (2.108 for **Ru1** and 2.107 Å for **Ru2**) as well as Ru–O bond distances (2.047 for **Ru1** and for **Ru2** for 2.056 Å) are comparable to those reported in the literature.[41] The torsional angle in homobimetallic **Ru1** is found to be 179.9° which is linear. Selected bond lengths and bond angles for both complexes are listed in Tables S6 and S7.†

Stability of complex Ru1

To understand the stability of the as-synthesised complex in water, crystals of **Ru1** were soaked in water for 24 h. In another experiment, **Ru1** was soaked in water and heated at 80 °C for 4 h. The powder X-ray diffraction pattern obtained for both these water-treated samples resembled that of the as-synthesized **Ru1**, thus confirming the stability of the **Ru1** complex (Fig. S5†).
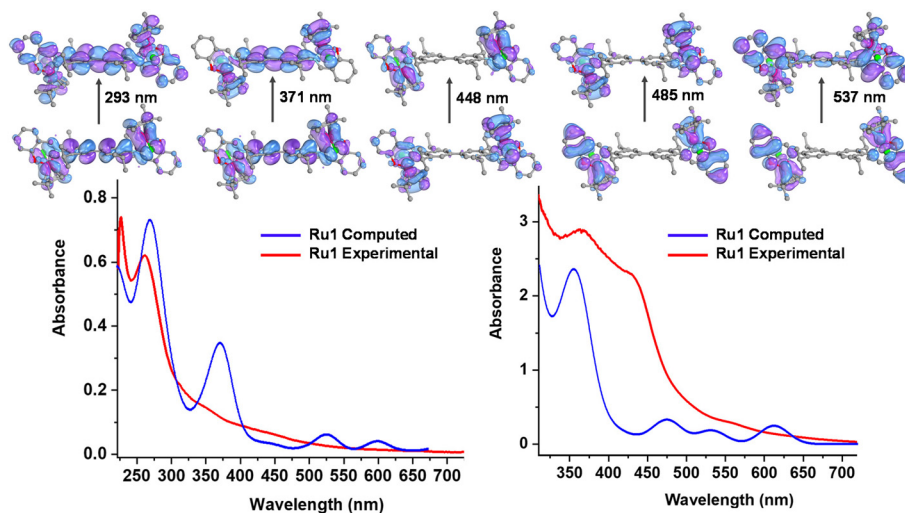

Fig. 1 UV−vis spectra of **Ru1** in dichlormethane at 4.52 x 10^{-3} M in the left and at 3.35 × 10^{-2} M in the right.
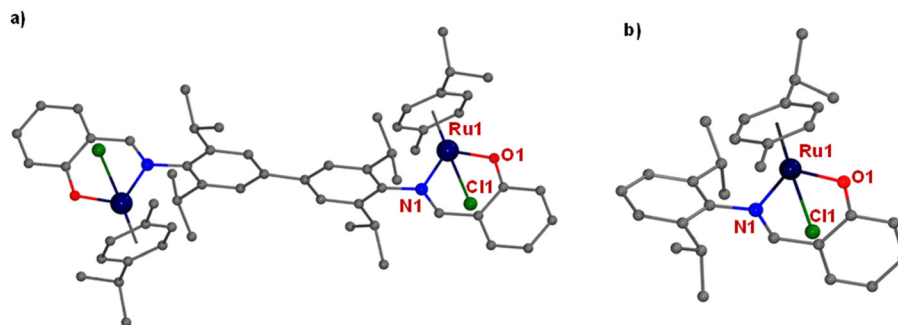
Fig. 2 Crystal structure of (a) **Ru1** and (b) **Ru2** complexes. Hydrogen atoms and solvent molecules are omitted for clarity. Selected bond lengths (Å) and bond angles (°) for **Ru1**: Ru(1)–Cl(1) 2.439(1), Ru(1)–O(1) 2.051(3), Ru(1)–N(1) 2.114(4), O(1)–Ru(1)–Cl(1) 83.5 (1), O(1)–Ru(1)–N(1) 86.8(1), and N(1)–Ru(1)–Cl(1) 84.8(1) and **Ru2**: Ru(1)–Cl(1) 2.4385(4), Ru(1)–O(1) 2.057(1), Ru(1)–N(1) 2.107(2), O(1)–Ru(1)–Cl(1) 82.99(4), O(1)–Ru(1)–N(1) 87.60(5), and N(1)–Ru(1)–Cl(1) 85.81(4). (Centroid of the *p*-cymene to Ru distance for **Ru1** and **Ru2** is 1.678 Å. For additional bond lengths and angles, see Tables S6 and S7.†

Reductive amination in water

To study the catalytic properties of the as-synthesized complexes, both catalysts were employed to produce secondary amines by RA. The reaction progress was monitored by NMR spectroscopy and GC-MS at regular intervals and isolated yields were calculated after the work-up of the reaction. The catalytic efficiency was determined using the TON and TOF after the completion of the reaction. Initially, a model reaction was carried out in water between benzaldehyde and aniline. Formic acid/formate buffer has been chosen for this study because it is mild and can offer more selectivity for the desired

Table 1 Optimisation of the reaction conditions for RA

Entry	**Ru1** Cat. (mol%)	Solvent	Buffer pH (3 mL)	Time (h)	Temp. (°C)	Yield[a] (%) a	b	c	Con.[b] (%)
1	2	H_2O	4.5	16	90	0	4	8	69
2	2	H_2O	4.2	16	90	9	11	17	78
3	2	H_2O	3.9	12	90	40	10	35	86
4	1	H_2O	3.7	12	90	64	8	14	90
5	0.2	H_2O	3.5	6	90	86	5	10	>99
6	0.1	H_2O	3.5	6	90	83	7	8	>99
7	0.05	H_2O	3.7	6	90	86	3	9	>99
8	0.05	H_2O	3.5	5	90	92	4	2	100
9	**0.05**	**H_2O**	**3.5**	**4**	**80**	**96**	**2**	**—**	**100**
10	0.05	H_2O	3.5	4	70	91	5	2	100
11	0.05	H_2O	3.5	4	60	86	8	5	100
12	0.05	H_2O	3.5	4	50	85	10	4	100
13	0.05	MeOH	3.5	4	70	62	25	—	86
14	0.05	Toluene	3.5	4	100	—	—	—	0
15	0.05	THF	3.5	4	100	23	47	—	73
16	0.05	^{i}PrOH	3.5	4	90	34	46	—	81
17[c]	0.1	H_2O	3.5	4	80	59	36	2	98
18	—	H_2O	3.5	4	80	—	99	—	99
19	0.05	H_2O	—	4	80	—	—	—	0
20[d]	0.05	H_2O	3.5	4	80	—	—	—	0
21	2	H_2O	3.5	4	80	59	—	36	>99
22	0.01	H_2O	3.5	4	80	81	18	—	>99
23	0.05	H_2O	3.0	4	80	62	7	—	100
24	0.05	H_2O	2.5	4	80	23	64	3	93
25	0.05	H_2O	2.0	4	80	10	81	—	92

Reaction conditions: benzaldehyde (1 mmol), aniline (1 mmol), solvent (2 mL), and HCOOH : HCOONa (3 mL). [a] Isolated yield. [b] Conversions were monitored using GC-MS. [c] Catalyst **Ru2** (0.1 mol%). [d] [Ru(*p*-cymene)RuCl$_2$]$_2$ (0.05 mol%).

products.[67] Optimisation conditions for various parameters are provided in Table 1. pH plays a crucial role in the RA reaction,[10,24,68–71] so the pH value of sodium formate buffer has been varied from 5.0 to 2.0. Results have shown that pH 3.5 is the best for RA with the **Ru1** complex. Furthermore, the catalyst loading, time, and temperature were optimized (Fig. 3). The best results were obtained with a catalyst loading of 0.05 mol% at pH 3.5 at 80 °C (4 h, Table 1, entry 9). A temperature of 80 °C makes the present RA catalytic system more viable and efficient than the earlier reported hydrogen borrowing amination methods.[18] The optimized reaction was also carried out with double the loading of an analogous monometallic **Ru2** complex as the catalyst (0.1 mol%), which gave 59% yield of the secondary amine (Table 1, entry 17). However, the reaction did not proceed when performed with the precursor [Ru(p-cymene)Cl$_2$]$_2$ as the catalyst (Table 1, entry 20).

The model reaction in methanol, isopropanol and tetrahydrofuran (THF) produced a poor yield of secondary amines, whereas the reaction did not yield the desired products when performed in toluene (Table 1, entries 13–16). This could be due to the fact that the use of a formic acid/formate system as the hydrogen source makes the entire catalytic system to be pH flexible. Thus, while aqueous conditions allow easy maintenance of a desired pH for maximum efficiency, the use of non-aqueous solvents/medium negates this advantage. In addition, the use of greener conditions such as using water and formate buffer is more eco-friendly than the use of toxic organic solvents such as toluene or THF. In the light of these obser-

vations, the optimal reaction conditions for RA have been chosen to be 0.05 mol% of **Ru1** in water with formic acid/formate (pH 3.5) as a hydrogen source at 80 °C for 4 h (Table 1, entry 9).

To comprehend the scope of the reaction, a large number of substrates (aldehydes and amines) were screened using the optimized reaction conditions (Table 1, entry 9). The effect of substituents on the reactivity and product formation was studied by varying the substituents either on aniline (Scheme 4) or aldehyde (Scheme 5). Anilines with electron-donating groups at the *para* position Me (**1b**), *^{t}*Bu (**1e**), *^{i}*Pr (**1d**), and OMe (**1c**) increase the yields (92–99%) as compared to *p*-electron-withdrawing substituents such as –F (**1f**), –Cl (**1g**) and –Br (**1h**) (90–93%). Anilines with *p*-NO$_2$ and *p*-CN do not proceed at all owing to the strong resonance effect of nitro and cyano groups. It is instructive to note that the **Ru1** catalyst performs well towards sterically hindered anilines such as 2,6-dimethyl aniline (**1o**) and 2,4,6-trimethyl aniline (**1p**) and also works well with aliphatic (**1l–1n**) and alicyclic amines (**1o**), as highlighted in Scheme 4. Aliphatic amines, owing to their low nucleophilicity and poor miscibility in water, result in sluggish formation of the imine intermediate which in turn reduces the efficiency of RA catalysis. Furthermore, the low hydrolytic stability of aliphatic imines is also one of the major factors for the low yield of secondary amines. For example, the formation energy of the aromatic imine from the corresponding amine is greater than the corresponding formation energy of the aliphatic imine, as confirmed by DFT calculations for substrates
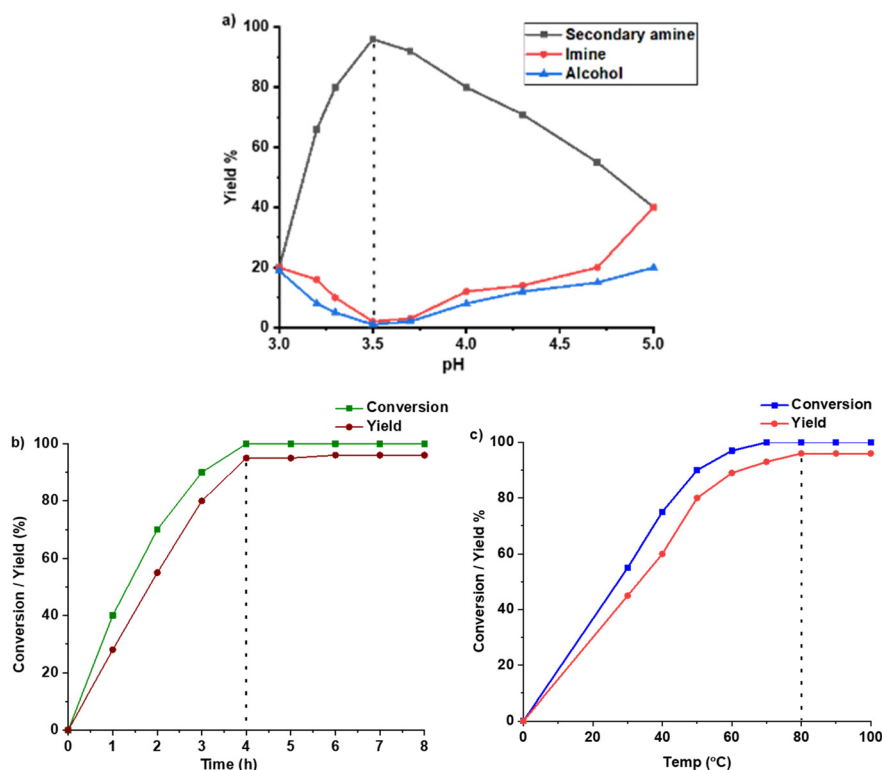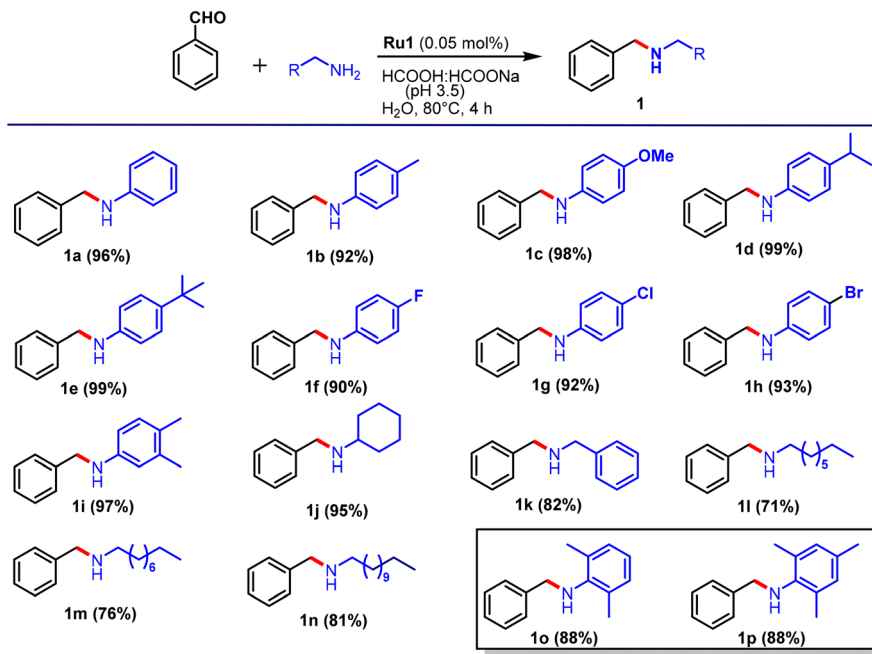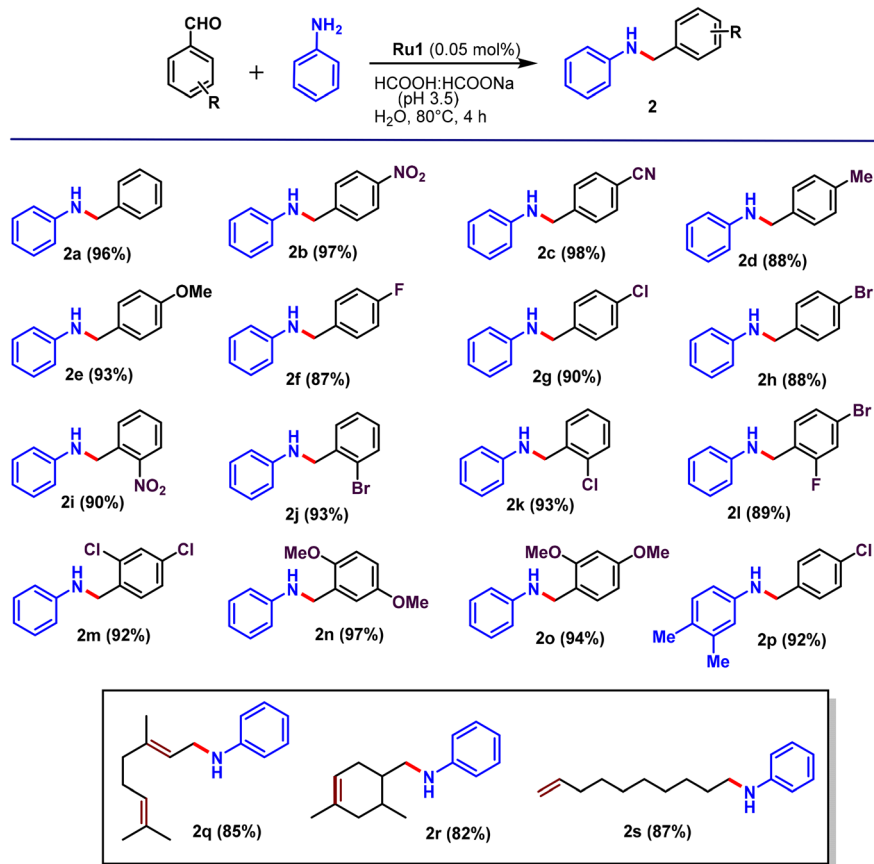

Fig. 3 Plot for the influence of the (a) pH value, (b) time, and (c) temperature on the formation of secondary amines.

Scheme 4 Substrate scope for amines with benzaldehyde for RA. Reaction conditions: benzaldehyde (1 mmol), amines (1 mmol), **Ru1** (0.05 mol%), HCOOH : HCOONa (3 mL, pH 3.5), water (2 mL), 80 °C for 4 h, isolated yield.


Scheme 5 Substrate scope for aldehydes with aniline for RA. Reaction conditions: aldehydes (1 mmol), aniline (1 mmol), **Ru1** (0.05 mol%), HCOOH : HCOONa (3 mL, pH 3.5), water (2 mL), 80 °C for 4 h, isolated yield.

1a and **1l**, which were found to be -32.3 kJ mol^{-1} and -5.8 kJ mol^{-1}, respectively (Fig. S22†).

Scheme 5 lists various aldehydes employed in the present study. The reactions involving benzaldehydes with electron-withdrawing substituents such as $-NO_2$ and $-CN$ at the *para* position as substrates exhibit enhanced yields (**2b** (97%), **2c** 99%) in comparison with the reactions involving electron-donating substituents (Me, **2d**, 88%, OMe, **2e**, 93%) on the benzaldehydes. The *para* halo-substituted benzaldehydes react in the following order Cl > Br > F (**2g** (90%), **2h** (88%), **2f** (87%)). However, the reactions involving disubstituted benzaldehydes produce the corresponding secondary amines in excellent yields (**2m** (92%), **2n** (97%), **2o** (94%), **2p** (92%)). A
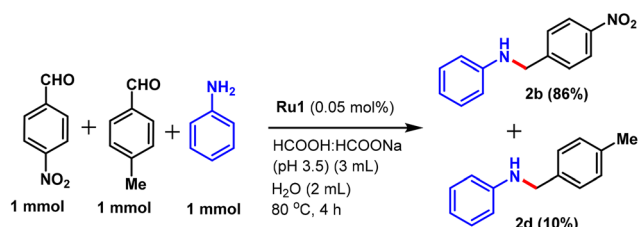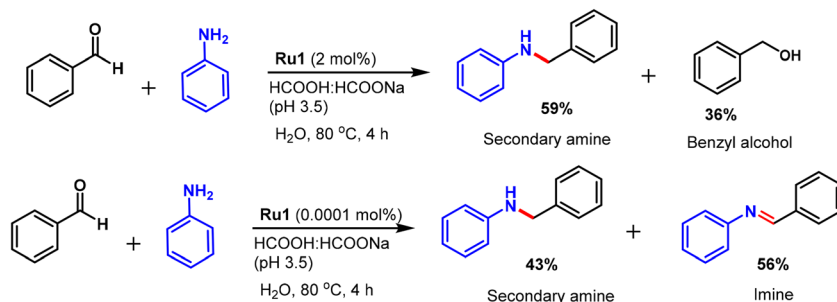

Scheme 6 Competitive experiments for aniline with benzaldehyde derivatives.
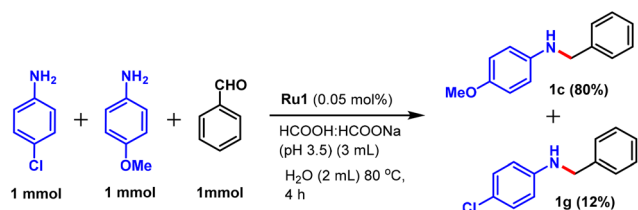
Scheme 7 Competitive experiments for benzaldehyde with aniline derivatives.
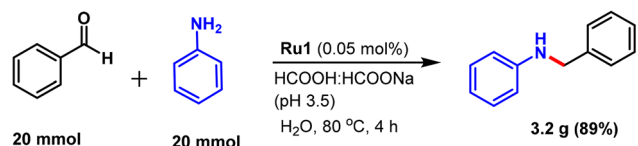

Scheme 8 Gram scale synthesis of secondary amines.

wide range of substrates having electron-withdrawing, electron-donating, nitro, cyano, and halo substituents on the aromatic rings remained unaltered under the said reaction conditions. Furthermore, to establish the chemoselectivity, unsaturated aldehydes and amines were studied. The presence of alkene groups in compounds such as citral, 2-(4,6-dimethyl-cyclohex-3-en-1-yl)acetaldehyde and undec-10-enal substrates makes selective RA challenging due to the possibility of hydrogenations over the alkene group. Interestingly, when the same substrate was reacted with aniline employing **Ru1** as a catalyst, a chemoselective RA occurred to yield the corresponding unsaturated secondary amines **2q–2s** in good yield.

Furthermore, two competitive experiments were carried out to emphasise the effect of substituents on the reactivity: (i) two different aldehydes *viz.* *p*-nitrobenzaldehyde (electron withdrawing group (EWG)) and *p*-toluidine (electron donating group (EDG)) were reacted with aniline in the same reaction vessel (Scheme 6) and (ii) two different anilines *viz.* *p*-chloroaniline (EWG) and *p*-anisidine (EDG) were reacted with benzaldehyde (Scheme 7) under the optimised conditions. From these experiments, it can be concluded that the electron-withdrawing substituents on the aldehyde and the electron donating functionalities on anilines promote the RA reaction. This can be attributed to faster nucleophilic attack of electron-rich anilines on the electron-deficient aldehyde to form the imine in the first step, which is then reduced by the catalyst in the further steps.

The catalytic efficiency of Ru1 for RA

The efficiency of catalyst **Ru1** was revealed in terms of TON and TOF calculated for the model reaction (benzaldehyde and aniline) under the optimized conditions which shows a TON of 1920 and a TOF of 480 h^{-1}. When the catalyst loading was reduced from 0.05 mol% to 0.0001 mol%, the highest TON and TOF of 4.3×10^4 and 107×10^3 h^{-1}, respectively, were observed. However, at this loading of the catalyst, the reaction suffers from lower selectivity for the secondary amine (43%, Table S1† entry 4) (also see Table S2† for the comparison of the reaction parameters of the present system with those of the reported effective catalyst for RA). It is important to highlight that the existing system can be used in large-scale reactions, as demonstrated by the success of RA in gram-scale reactions with **Ru1**. As shown in Scheme 8, the reaction of aniline

Scheme 9 Control experiments with **Ru1**.
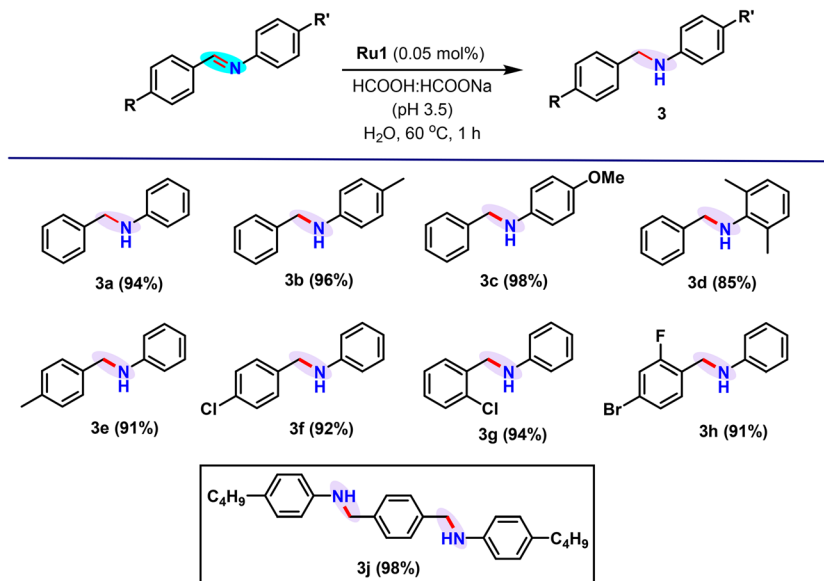
Scheme 10 Substrate scope for imine reduction. Reaction conditions: imine (1 mmol), (0.05 mol%), HCOOH : HCOONa (3 mL, pH 3.5), water (2 mL), temperature 60 °C for 1 h, isolated product yield.

(20 mmol) with benzaldehydes (20 mmol) under optimal reaction conditions using 0.05 mol% catalyst produced the desired secondary amine in 89% yield (3.2 g).

Green metrics analyses additionally revealed high atom economy (91.97%), atom efficiency (81.85%) and reaction mass efficiency (82.05%) for the gram-scale reaction, demonstrating that RA with the **Ru1** catalyst is an atom-efficient method.[72] Moreover, this reaction only generates water as a byproduct (see Table S3† for a comparison of the green metrics of the present system with earlier reported catalysts for RA). This experiment coupled with the aforementioned TONs and TOFs demonstrates the practicality and high efficiency of RA catalysed by **Ru1**.

The abovementioned results demonstrate that the present bimetallic catalytic system is able to achieve chemoselectively high yield of secondary amines even with a lower catalyst loading of 0.05 mol% (**Ru1**). The use of formate buffer as an alternate source of hydrogen in an aqueous medium makes it greener and more sustainable with high green metrics.

Control experiments and mechanistic investigation

A series of control experiments were carried out to explain the mechanistic pathway of RA. The reaction of benzaldehyde with aniline was performed at various catalyst concentrations to understand the effect of catalyst loading on the selectivity of the product (or the side products mentioned in Table 1). As mentioned above, the optimum catalyst loading for RA is 0.05 mol% of **Ru1**. However, when the catalyst loading was increased to 2 mol%, the reaction time reduced to 2 h, but this resulted in poor selectivity of the secondary amine (59%), with increased formation of alcohol as a side product (Scheme 9; also see Table 1, entry 21). On the other hand, the lowering of the catalyst loading to 0.0001 mol% led to a decrease in the for-

mation of the secondary amine (43%) and an increase in the yield of an imine (56%) as a side product (Scheme 9; Table S1,† entry 4). Furthermore, control experiments conducted in the
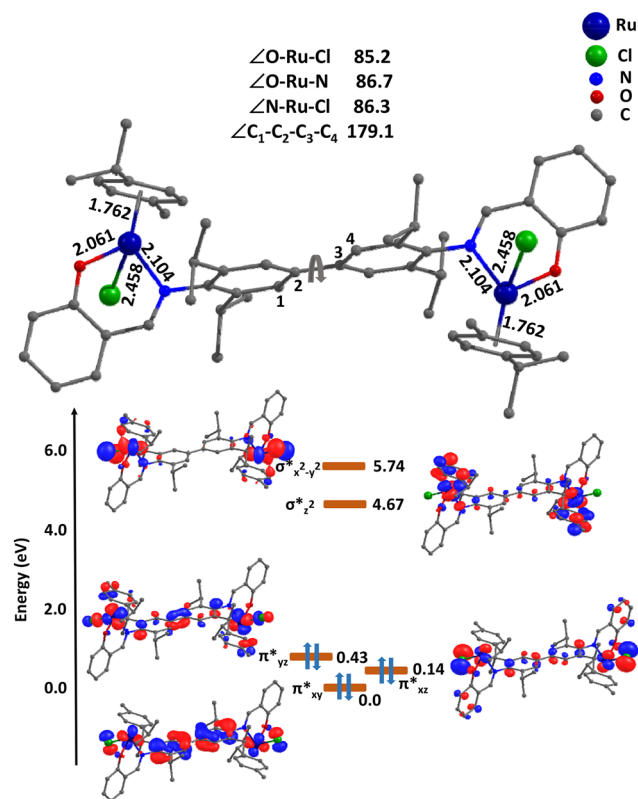
Fig. 4 The computed B3LYP-D2 (top) optimised structural parameters for **Ru1** and (bottom) eigenvalue plot for d-orbitals plotted using an iso-surface value of 0.035.

absence of a catalyst yielded only an imine, with no secondary amine product being produced (Table 1, entry 18).

As we have mentioned above, the formation of alcohol as a side product can be significantly influenced by an increased catalyst loading (*i.e.* 2 mol%) and it can also be altered by the pH of formate buffer. This occurs because the formation of an imine or alcohol is initially a competitive reaction. When the catalyst concentration is higher, the formation of alcohol is favoured due to the high rate of the reaction. However, at a low pH the carbonyl group is better activated due to protonation, resulting in high alcohol formation.

Using earlier reports and experimental observation, the mechanism for alcohol formation can be demonstrated as follows.[67,73] As shown in the catalytic cycle (Scheme S4†), in the first step, a chloride ion is replaced by formate, resulting in the formation of ruthenium formato species **II**. Subsequently, intermediate **II** undergoes β-hydride elimination to produce ruthenium hydride species **III**. After that, the carbonyl substrate coordinates with species **III**, and hydride transfer occurs on activated carbonyl to produce alcohol as a product and thereby complete the catalytic cycle.

To investigate the formation of the imine (C=N) intermediate and its successive reduction by the catalyst **Ru1**, a pre-syn-thesized imine (from benzaldehyde and aniline; a trial reaction) was converted *in situ* to an amine under the optimal reaction conditions (Table 1, entry 9), resulting in excellent yields of a secondary amine. However, while monitoring the reaction, we found that imine conversion was completed within 1 h of the reaction time. As a result, we have investigated the reduction of imines to secondary amines at a lower reaction temperature and time (60 °C and 1 h, respectively) for various substrates (Scheme 10). The large number of imine substrates including both electron-rich and electron deficient were transformed to the corresponding secondary amines using the **Ru1** catalyst in good yield. These results conclude that the homobimetallic catalyst **Ru1** is highly effective and selective for the conversion of aldehydes, amines including aromatic, aliphatic, and alicyclic, and imines to secondary amines. Also, all of the above experiments suggest that 0.05 mol% of catalyst with formate/formic acid buffer (pH 3.5) is essential for the complete conversion of aldehydes and anilines (as well as imines) to secondary amines in good yields.

Mechanistic studies

The optimised geometry along with the corresponding eigenvalue plot for the **Ru1** system is given in Fig. 4. The geometry
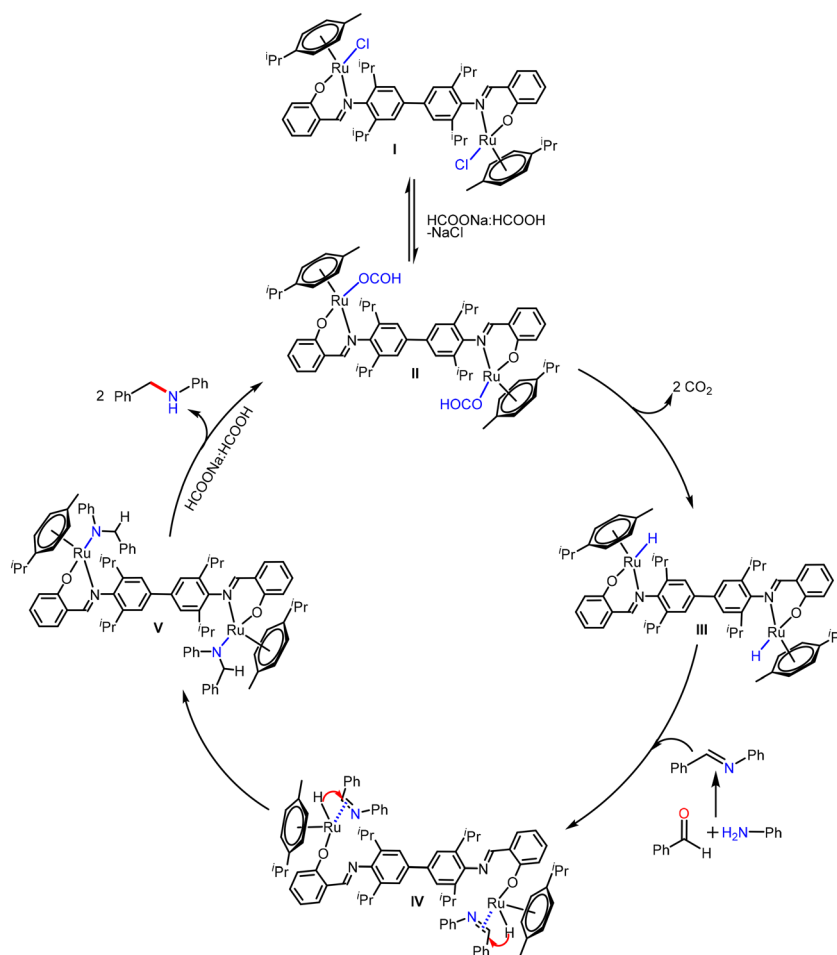
Scheme 11 Proposed mechanism for RA with the **Ru1** catalyst.

around Ru(II) is strongly distorted octahedral which is reflected in the lifting of the degeneracy of the t_{2g} set of orbitals with the d_{xy} orbital stabilised and the π-donor –Cl ligand further lifting the degeneracy between the d_{xz} and d_{yz} orbitals (0.29 eV). Due to the very strong ligand field, the Ru t_{2g} and e_g orbital gap $\Delta(E_{\sigma*z2} - E_{\pi*yz})$ is estimated to be 4.23 eV with the $(d_{xy})^2(d_{xz})^2(d_{yz})^2(d_{x_2-y_2})^0(d_{z_2})^0$ electronic configuration (Fig. 4).

We have adopted the following mechanism for the RA reaction based on the previously reported mechanisms for similar reactions and our experimental and theoretical findings (Scheme 11).[15,29,74,75] To begin with, the Ru–Cl bond is expected to be replaced by the formate ion, and we have considered (i) a dissociative mechanism where the Ru–Cl bond cleaves in the first step leading to a five-coordinate intermediate followed by the formate binding. The formation of a low-coordinate intermediate is found to be endothermic by 88.8 kJ mol⁻¹. The optimised geometry of the (**I-II$_{p1}$**) intermediate reveals a strong donation of *p*-cymene to Ru, upon the departure of –Cl and significant reorganisation of the geometry around Ru, which contribute to the observed endothermicity; (ii) an associative mechanism where the simultaneous replacement of –Cl by a formate ion is envisioned, and (**I-II$_{p2}$**) formation of this species is found to be exothermic by −142.6 kJ mol⁻¹. A closer inspection of the optimized geometry reveals that this is also a six-coordinate species with the Ru–N bond of

the chelate ring elongated significantly to accommodate the formate insertion, suggesting a flexible coordination sphere offered by the Schiff-base ligand during the reaction. The binding of the formate ion and departure of –Cl lead to the formation of species **II**, which has also been computed to be significantly exothermic (−231.2 kJ mol⁻¹) (Fig. 5). Such a facile formation suggests the stability for this species and is affirmed by the experiments with the detection of the peak corresponding to this species in the ESI-MS spectrum at *m/z* 1121.29 (Fig. S14†). In the next step, CO₂ elimination is expected to occur *via* β-hydride transfer, triggering the formation of Ru–H species (**III**), the formation of which is found to be exothermic by 16.8 kJ mol⁻¹, from species **II**, suggesting facile formation. This step is favoured by the proximity of the H atom of the formate to Ru (H⋯Ru at the species **II** is 2.97 Å) to enable the formation of Ru–H species. This species is also detected by ESI-MS at *m/z* 1033.32 (Fig. S15†), offering confidence in the proposed mechanism.

In the next step, the imine formed from the condensation reaction is expected to enter the catalytic cycles and coordinate with the Ru centres (species **IV**). For this coordination to occur, the linked nitrogen atom in the Schiff-base ligand undergoes dissociation, eventually resulting in the establishment of a potent η² bond with the C=N group of the imine. As this involves cleavage of the Ru–N bond and the formation of the Ru–
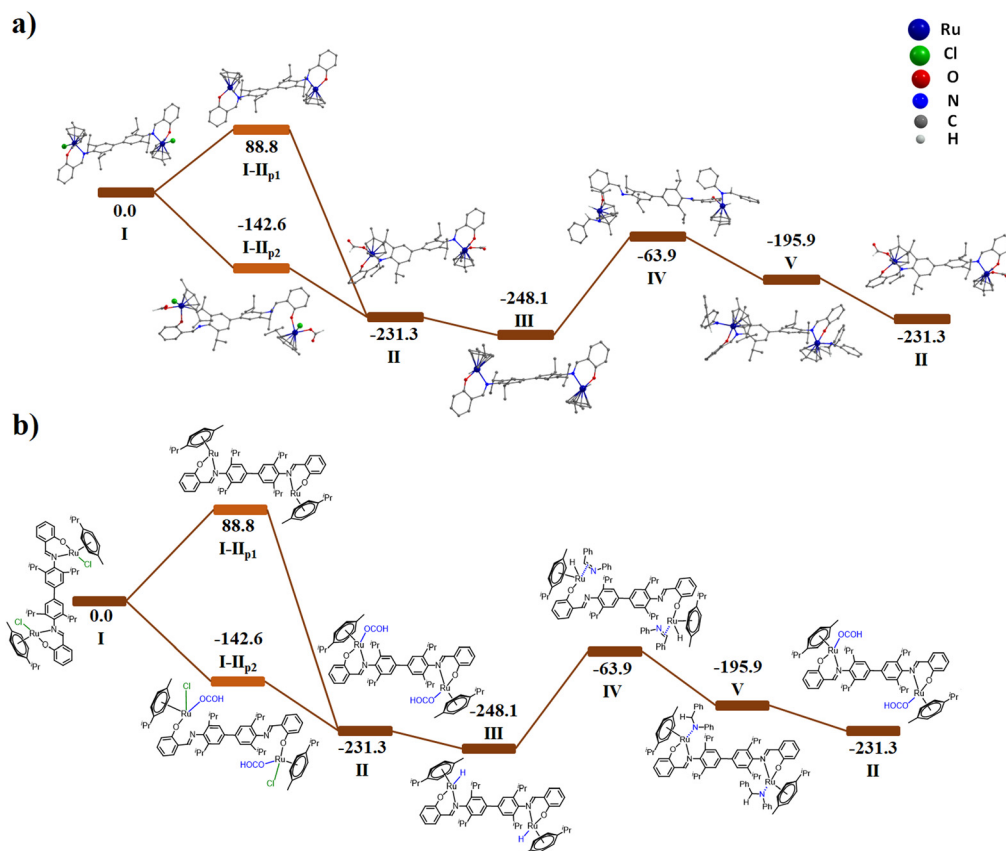

Fig. 5 (a) The computed potential energy profile diagram in solvent phase free energies (ΔG), at the B3LYP-D3/def2-TZVP level of theory for reaction pathways of the bimetallic complex for **I** to **V**. (b) The corresponding Chemdraw energy profile.

η^2(Ph–C=N–Ph) bond, this is found to be endothermic from species **III** by 184.2 kJ mol^{-1}. However, from the reactants, the formation is exothermic by −63.9 kJ mol^{-1}. In the next step, hydride migration to the carbon atom of the coordinate imine is expected, leading to the formation of species **V**, and this is facilitated at species **III** with the short H···C(imine) of 2.244 Å. The formation of species **V** is exothermic by 132.0 kJ mol^{-1} from species **IV**, suggesting facile hydride transfer. In the next step, the nitrogen of the coordinated imine will be protonated from the acid buffer that is added in the reaction leading to the release of the product and the regeneration of the species **II** whose formation is also exothermic, suggesting a facile reaction.

The effect of pH on the rate of transfer hydrogenation of ketones and quinolines has been previously studied by J. Xiao and co-workers which suggests that the formation of an active catalyst is facilitated at a particular pH value.[67,76–79] To gain an insight into the pH dependence of the mechanism, we have compared our experimental results with mechanistic pathways reported in the literature.[10,76] As shown in Fig. 6, the pH of buffer has a strong influence on the RA reaction, with the highest yield being observed at pH 3.5. At a low pH, the concentration of the reductant is low due to the decomposition of HCOO$^-$ into CO_2 and HCO$_3^-$. At a higher pH, the concentration of the active catalyst Ru-formate (intermediate **II**) is low.[78] However, at an intermediate pH of 3.5, the concentration of both the reductant and the active catalyst Ru-formate is the highest, which then results in the highest rate of secondary amine formation (Fig. 6).

Comparative study of homobimetallic (Ru1) and monometallic (Ru2) catalysts

Attempts have also been made to compare the reactivity of one *versus* two metal centers for both complexes, **Ru1** and **Ru2**. The comparison of potential energy has given evidence for the segregation of **Ru1** and **Ru2** reactivity (see Fig. S19 and S21,† respectively). It has also been observed that the reactivity
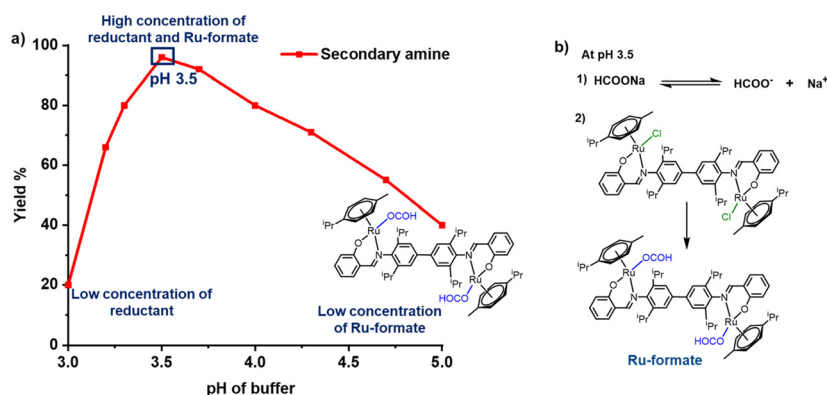

Fig. 6 (a) The variation of the yield of the secondary amine as well as Ru-formate to change in the pH of formate buffer. (b) Formation of Ru-formate at pH 3.5.
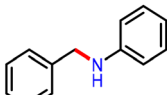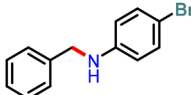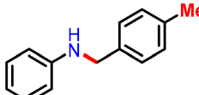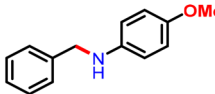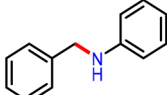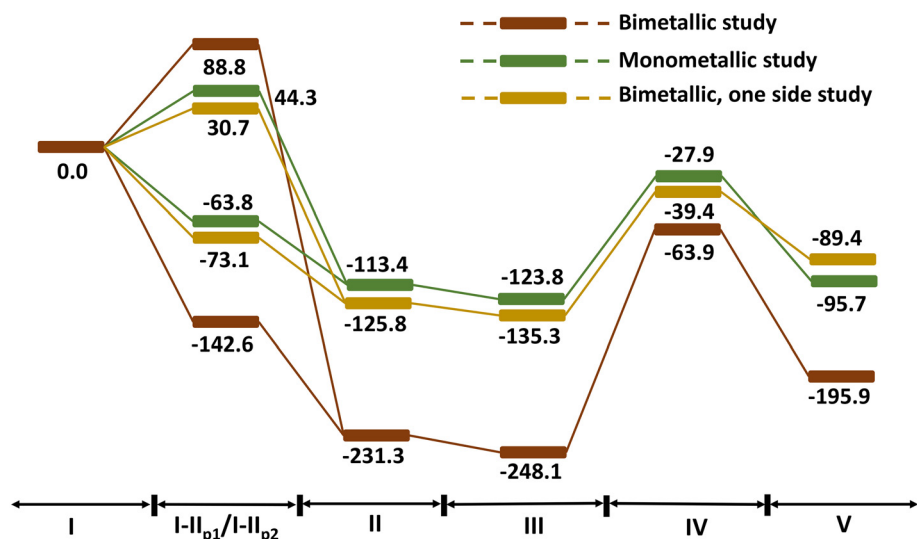

Fig. 7 The computed potential energy profile diagram in solvent phase free energies (ΔG in kJ mol^{-1}), bimetallic complex, monometallic and bimetallic model with only one Ru being reactive for **I** to **V**.

pattern for **Ru1** has more stability in each intermediate, and the statistical probability is also higher for the dimer since it contains two active metal centers. Experimentally, a reaction between benzaldehyde and aniline was carried out under identical optimized reaction conditions; however, **Ru2** was loaded at 0.1 mol% (since it is monometallic). Interestingly, **Ru1** produced a secondary amine as the major product (96%) and an imine as a minor product (3%). Similarly, **Ru2** resulted in the formation of similar products, but the product ratio varied (secondary amine 59% and imine 36%).

Table 2 Substrate scope for amines and benzaldehyde for RA with **Ru2**

| Entry | Secondary amine | Yield of secondary amine (yield of imine) (%) | |
| | | Catalyst | |
		Ru1	**Ru2**
1		96 (2)	59 (36)
2		93 (6)	64 (27)
3		92 (7)	56 (39)
4		98 (0)	70 (24)
5[a]		96 (2)	71 (25)

Reaction conditions: benzaldehyde (1 mmol), amines (1 mmol), **Ru1** (0.05 mol%), **Ru2** (0.1 mol%), HCOOH : HCOONa (3 mL, pH 3.5), water (2 mL), 80 °C for 4 h, isolated yield. [a] **Ru2** (1 mol%); imine yield (%) is given in parentheses.

Along with these experimental and computational calculations, we have modeled a catalyst in which one Ru center participates in the reaction and the second metal center is considered to be in the inactive state. It is clear from these calculations that the formation of species **II–V** is facilitated and faster when both the Ru centres are reacting simultaneously with the energy margin of 4.5, 0.5, 8.1 and 4.5 kJ mol^{-1} for species **II–V**, respectively. The largest energetic gain is witnessed for species **IV** which is the only endothermic step noticed in the reaction. The calculations performed using dimeric model but keeping only one of the Ru metal as the active centre for the catalytic reaction found to yield energies which are relatively more exothermic compared to monomeric models (Fig. 7). Thus, dinuclear Ru centres offer both structural and electronic cooperativity during the course of the reaction to facilitate product selectivity.[91]

To comprehend the cooperativity in **Ru1**, we have considered more selected substrates, including electron-donating substituents, *viz.* *p*-Me and *p*-OMe, and electron-withdrawing substituents *viz.* *p*-Br, which were found to have similar reactivity patterns. Even when the catalyst loading of **Ru2** was increased from 0.1 mol% to 1 mol%, a secondary amine:imine ratio of 3 : 1 was observed (Table 2). This difference in the product ratio suggests that the homobimetallic catalyst is highly active and forms ruthenium hydride species faster (**III** in a catalytic cycle). This quick precatalyst activation can be attributed to the cooperative interaction between two metals in **Ru1**, which is absent in the monometallic catalyst **Ru2**.

Detection of intermediates II and III by ESI-MS

Ru1 (0.01 mmol) was mixed with 2.0 mL of water along with 3.0 mL of buffer (HCOOH : HCOONa, pH 3.5) and heated at 60 °C in a round bottom flask. Once the reaction started, an aliquot was taken at an interval of every five minutes and analyzed by mass spectrometry. The Ru-formate species **II** was identified at *m/z* 1121.299 after ten minutes; this species immediately changed into Ru-hydride species **III**, which was also detected by mass spectrometry at *m/z* 1033.325 (Fig. 8). A prominent change in color from pale yellow to brown in the
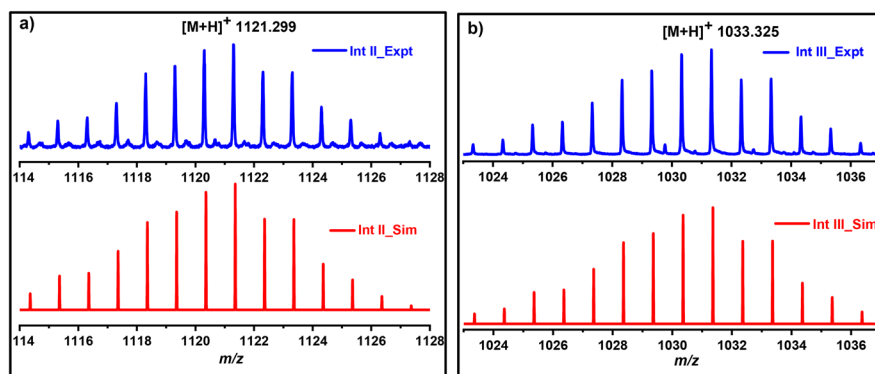

Fig. 8 ESI-MS spectra showing the experimental and simulated isotopic patterns of the [M + H]$^+$ ion peak for (a) intermediate **II** and (b) intermediate **III** in methanol.

reaction mixture was observed once the species converted from Ru-formate to the Ru-hydride intermediate.

Conclusion

Homobimetallic Ru(II) complex **Ru1** by far is the most effective catalyst for the selective one-pot RA of aldehydes in the aqueous medium. Starting from inexpensive aldehydes and amines, we have showcased in the present work that **Ru1** based RA can produce functionalised and structurally varied secondary amines with high TONs and TOFs even in water. Unlike in many of the previous reports for RA, the present methodology neither requires high pressure nor the use of hydrides; the reaction also does not generate waste that is harmful to the environment. In RA processes, it may often become difficult to achieve chemoselectivity; in this sense, our uncomplicated approach based on the homobimetallic Ru(II) complex **Ru1** offers a remarkable demonstration of RA of complicated and functionalized compounds. The question of a bimetallic *versus* a monometallic system for improved efficiency and selectivity has been successfully addressed with the aid of DFT studies on the possible reaction pathways and intermediates.

Experimental section

Computational details

All DFT calculations have been performed in the Gaussian16.C suite of programs.[92] The methodology that has been used is B3LYP-D3 functional along with the basis set SDD for Ru atoms and 6-31G*[80,81] for other atoms. This is a time-tested methodology for the Ru catalyst and also has reproduced several experimental spectral features,[82] offering confidence in the methodology. The single point energies were computed on the optimized geometries with the def2-TZVP basis set for all atoms.[83] The Gibbs free energy correction has been added to the single point energies obtained from the higher basis set to refine the gas phase electronic energies. The solvation has been modeled using the polarisable continuum model (PCM), using water as the solvent.[84] The geometrical parameters obtained from the optimized structure of catalysts **Ru1** and **Ru2** are in agreement with the single-crystal X-ray diffraction data (ESI, Fig. S16, S17, and Table S4†). The Natural Bonding Orbitals (NBO) analysis has been performed with the same methodology.[85] Time-dependent TD-DFT was carried out using the ORCA5.0.4 software package[86–89] using the B3LYP-D3/def2-TZVP setup in dichloromethane solvent using a conductor-like polarizable continuum model (CPCM) solvation model along the resolution of the identity (RI-JK) approximation.[90]

Materials and methods

All the experimental procedures were conducted in a well-ventilated fume hood under an ambient atmosphere. The starting material 2,2′,6,6′-tetraisopropylbenzidine, Schiff-base ligands **H₂L¹** and **HL²**, 4-bromo-2,6-di-iso-propylaniline, and [Ru(*p*-cymene)(μ-Cl)Cl]₂ were prepared according to the reported procedures.[62,63] The starting materials like ruthenium(III)trichloride trihydrate, α-phellandrene, salicylaldehyde (Sigma Aldrich), bromine (Spectrochem), and 2,6-diisopropylaniline (Alfa Aesar) procured from commercial sources were used as received. Similarly, the amine and aldehyde substrates employed in catalysis were procured from commercial sources. The ruthenium compounds reported herein are air and moisture stable, and hence, no special measures were taken to preclude air and moisture during their manipulation.

Physical measurements and instruments

The ¹H and ¹³C NMR spectra were recorded either on a Bruker Avance III 500 or Bruker AV III 400 MHz NMR spectrometer using CDCl₃ or DMSO-d₆ as solvents. The melting points were measured in glass capillaries and are reported uncorrected. FT-IR spectra were recorded on a PerkinElmer Spectrum One Infrared Spectrometer (model number - 73465) in KBr diluted discs within the 4000–400 cm⁻¹ frequency range. Elemental analyses were performed on a Thermo Finnigan (FLASH EA 1112) microanalyser. ESI-MS measurements were performed on a Bruker Maxis Impact electrospray mass spectrometer. A UV-NIR-3600 spectrophotometer (Shimadzu) was used for the UV-visible studies. Powder X-ray diffractions were recorded on a Rigaku SmartLab powder X-ray diffractometer using Cu-Kα radiation (λ = 1.54190 Å). The molecular structures of complexes **Ru1** and **Ru2** were determined using Mo-Kα radiation (λ = 0.71073 Å) and a Bruker D8 QUEST diffractometer.[93–96] An Agilent 7890A GC system with an FID detector and a J & WDB-1 column (10 m, 0.1 mm ID) was used to conduct GC-MS analysis; the catalytic product yields of the optimized reactions were determined for one of the starting materials.

Synthesis of the [(*p*-cymene)₂(RuCl)₂L¹] complex (Ru1)

Schiff-base **H₂L¹** (2,2′-((1*E*,1′*E*)-((3,3′,5,5′-tetraisopropyl-[1,1′-biphenyl]-4,4′-diyl)bis(azaneylylidene))bis(methaneylylidene)) diphenol) (112 mg, 0.2 mmol) and potassium carbonate (0.4 mmol, 56 mg) were mixed in ethanol (50 mL), and to this mixture, the metal precursor [Ru(*p*-cymene)(μ-Cl)Cl]₂ (0.20 mmol, 122 mg) was added under stirring. The reaction mixture was stirred vigorously overnight at room temperature. The colour of the reaction mixture changed from yellow to dark red indicating the progress of the reaction. After 12 h, the solvent was removed under vacuum to obtain crude product **Ru1** in the form of a red residue. This residue was dissolved in dichloromethane and filtered through Celite to obtain pure ruthenium cymene complex **Ru1** in high yield. **Ru1** was purified by recrystallisation from an ethanol : dichloromethane (1 : 4 v/v) mixture as dark red crystals. Yield (164 mg, 75%) mp. > 250 °C. Anal. cal. for C₅₈H₇₀N₂O₂Cl₂Ru₂; C, 63.32; H, 6.60; N, 2.51. Found: C, 62.79; H, 6.74; N, 2.10; ESI-MS: [M − Cl]⁺ = 1065.307 *m/z* (M_r = 1100.292); ¹H NMR (400 MHz, CDCl₃) δ 8.39 (s, 2H), 7.61 (s, 2H), 7.55 (s, 2H), 6.99 (d, $^3J_{H,H}$ = 8.57 Hz, 2H), 6.89 (t, $^3J_{H,H}$ = 7.27 Hz, 2H), 6.45 (d, $^3J_{H,H}$ = 8.56 Hz, 2H), 5.49 (d, $^3J_{H,H}$ = 6.13 Hz, 2H), 5.40 (d, $^3J_{H,H}$ = 6.19 Hz, 2H), 5.00

(d, $^3J_{H,H}$ = 5.64 Hz, 2H), 4.38 (d, $^3J_{H,H}$ = 5.65 Hz, 2H), 3.28 (sept, $^3J_{H,H}$ = 6.82 Hz, 2H), 3.13 (sept, $^3J_{H,H}$ = 6.82 Hz, 2H), 2.85 (sept, $^3J_{H,H}$ = 6.75 Hz, 2H), 2.06 (s, 6H) 1.59 (d, $^3J_{H,H}$ = 7.03 Hz, 6H), 1.51 (d, $^3J_{H,H}$ = 6.82 Hz, 6H), 1.42 (d, $^3J_{H,H}$ = 7.12 Hz, 6H), 1.32 (d, $^3J_{H,H}$ = 6.71 Hz, 6H), 1.16 (d, $^3J_{H,H}$ = 6.83 Hz, 6H), 1.13 (d, $^3J_{H,H}$ = 6.65 Hz, 6H) ppm. ^{13}C NMR (101 MHz, CDCl$_3$): δ 166.87, 152.20, 143.44, 142.32, 135.61, 134.97, 122.99, 122.02, 119.36, 114.63, 94.47, 87.70, 84.48, 82.03, 30.75, 26.13, 23.42, 17.86 ppm. FT-IR (KBr diluted Pellet, cm^{-1}) 2960, 1610, 1523, 1444, 1331, 1240, 1141, 809, 615; UV-Vis (DCM, λ_{max} (nm), ε ($\times10^5$ M^{-1} cm^{-1})) 226 (1.6), 266 (1.3).

Synthesis of the [(p-cymene)(RuCl)L^2] complex (Ru2)

Ru2 was synthesised as mentioned above using Schiff-base **HL^2** (2,6-(((diisopropylphenyl)imino)methyl)phenol) (0.4 mmol, 112 mg) and potassium carbonate (0.4 mmol, 56 mg) and [Ru (p-cymene)(μ-Cl) Cl]$_2$ (0.2 mmol, 122 mg). Yield (171 mg, 77%) mp. > 250 °C. Anal. cal. for C$_{29}$H$_{36}$NOClRu. C, 63.20; H, 6.58; N, 2.54. Found: C, 62.95; H, 6.64; N, 2.20; ESI-MS: [M − Cl]$^+$ = 516.198 m/z (M$_r$ = 551.13); ^{1}H NMR (400 MHz, CDCl$_3$) δ 7.48 (s, 1H), 7.35 (d, $^3J_{H,H}$ = 6.13 Hz, 1H), 7.32–7.30 (m, 1H), 7.20–7.17 (m, 1H) 6.96 (d, $^3J_{H,H}$ = 8.54 Hz, 1H), 6.85 (dd, $^3J_{H,H}$ = 8.53 Hz, 8.51 Hz, 1H), 6.44 (d, $^3J_{H,H}$ = 7.0 4 Hz, 1H), 5.43 (d, $^3J_{H,H}$ = 5.45 Hz, 1H), 5.31 (d, $^3J_{H,H}$ = 7.04 Hz, 1H), 4.94 (d, $^3J_{H,H}$ = 5.48 Hz, 1H), 4.26 (d, $^3J_{H,H}$ = 5.48 Hz, 1H), 3.18 (sept, $^3J_{H,H}$ = 7.25 Hz, 1H), 2.81 (sept, $^3J_{H,H}$ = 7.18 Hz, 1H), 1.98 (s, 3H), 1.48 (d, $^3J_{H,H}$ = 7.10 Hz, 3H), 1.37 (d $^3J_{H,H}$ = 7.23 Hz, 6H), 1.29 (d, $^3J_{H,H}$ = 6.84 Hz, 3H), 1.07 (d, $^3J_{H,H}$ = 6.65 Hz, 3H), 1.02 (d, $^3J_{H,H}$ = 6.65 Hz, 3H) ppm. ^{13}C NMR (101 MHz, CDCl$_3$): δ 166.59, 152.59, 142.63, 142.32, 135.61, 134.97, 122.99, 122.02, 119.36, 114.63, 94.47, 87.70, 84.48, 82.03, 30.75, 26.13, 23.42, 17.86 ppm. FT-IR (KBr diluted Pellet, cm^{-1}) 2990, 1630, 1533, 1424, 1341, 1239, 1150, 801, 619; UV-Vis (DCM, λ_{max} (nm), ε ($\times10^4$ M^{-1} cm^{-1})): 230 (7.2), 261 (6.8) 311 (1.7).

General procedure for RA catalysis

An oven-dried round bottom flask containing a stir bar was charged with aldehydes (1.0 mmol), amines (1.0 mmol), and water (2.0 mL) and stirred under an ambient atmosphere for 5 minutes. **Ru1** (0.05 mol%) and buffer solution (HCOOH : HCOONa, pH 3.5, 3 mL) were added to the reaction mixture. The resultant reaction mixture was stirred at 80 °C for 2–5 h. After completion of the reaction, the product was extracted with ethyl acetate and dried over sodium sulphate. The secondary amines formed by this method were further purified by column chromatography (petroleum ether medium : ethyl acetate 98 : 2) and analysed by NMR spectroscopy.

Following the same procedure, RA using **Ru2** (0.1 mol%) as a catalyst was carried out to compare the catalytic activity with **Ru1**.

General procedure for reduction of C=N bonds

A round bottom flask equipped with a stir bar was charged with aldehyde and amine substrates (1.0 mmol) in water (2.0 mL) and stirred in an open atmosphere at 60 °C for 35–40 minutes. Upon confirming imine formation by GC-MS analysis, **Ru1** (0.05 mol%) and buffer solution (HCOOH : HCOONa, pH 3.5,

3 mL) were added to the reaction mixture and stirred at 60 °C for 1 h. After completion of the reaction, the product was extracted with ethyl acetate and dried over sodium sulphate. The secondary amines formed by this catalysis method were further purified by column chromatography if required (petroleum ether medium : ethyl acetate in 98 : 2 ratio) and analysed by NMR spectroscopy.

Conflicts of interest

There are no conflicts to declare.

Acknowledgements

References

1 S. Kobayashi and H. Ishitani, *Chem. Rev.*, 1999, **99**, 1069–1094.

2 V. Froidevaux, C. Negrell, S. Caillol, J. P. Pascault and B. Boutevin, *Chem. Rev.*, 2016, **116**, 14181–14224.

3 K. S. Hayes, *Appl. Catal., A*, 2001, **221**, 187–195.

4 O. I. Afanasyev, E. Kuchuk, D. L. Usanov and D. Chusov, *Chem. Rev.*, 2019, **119**, 11857–11911.

5 M. S. Thakur, O. S. Nayal, A. Sharma, R. Rana, N. Kumar and S. K. Maurya, *Eur. J. Org. Chem.*, 2018, 6729–6732.

6 F. D. Klingler, *Acc. Chem. Res.*, 2007, **40**, 1367–1376.

7 D. Quo, H. Huang, J. Xu, H. Jiang and H. Liu, *Org. Lett.*, 2008, **10**, 4513–4516.

8 J. Wu and C. Darcel, *ChemCatChem*, 2022, **14**, e202101874.

9 Y. Pan, Z. Luo, X. Xu, H. Zhao, J. Han, L. Xu, Q. Fan and J. Xiao, *Adv. Synth. Catal.*, 2019, **361**, 3800–3806.

10 C. Wang, A. Pettman, J. Basca and J. Xiao, *Angew. Chem.*, 2010, **122**, 7710–7714.

11 R. Xie, C. Liu, R. Lin, R. Zhang, H. Huang and M. Chang, *Org. Lett.*, 2022, **24**, 5646–5650.

12 Z. Wu, H. He, M. Chen, L. Zhu, W. Zheng, Y. Cao and J. C. Antilla, *Org. Lett.*, 2022, **24**, 9436–9441.

13 V. Kumar, S. Sharma, U. Sharma, B. Singh and N. Kumar, *Green Chem.*, 2012, **14**, 3410–3414.

14 C. Kerner, S. D. Straub, Y. Sun and W. R. Thiel, *Eur. J. Org. Chem.*, 2016, 3060–3064.

15 İ. K. Özbozkurt, D. Gülcemal, S. Günnaz, A. G. Gökçe, B. Çetinkaya and S. Gülcemal, *ChemCatChem*, 2018, **10**, 3593–3604.

16 A. R. Fatkulin, O. I. Afanasyev, A. A. Tsygankov and D. Chusov, *J. Catal.*, 2022, **405**, 404–409.

17 V. R. Jumde, L. Gonsalvi, A. Guerriero, M. Peruzzini and M. Taddei, *Eur. J. Org. Chem.*, 2015, 1829–1833.

18 E. Podyacheva, O. I. Afanasyev, D. V. Vasilyev and D. Chusov, *ACS Catal.*, 2022, **12**, 7142–7198.

19 E. W. Baxter and A. B. Reitz, *Organic Reactions*, John Wiley & Sons, Inc., 2002, 59, pp. 1–714.

20 P. M. Illam and A. Rit, *Catal. Sci. Technol.*, 2022, **12**, 67–74.

21 Y. Wang, F. L. Zhang, Z. J. Liu and Z. J. Yao, *Inorg. Chem.*, 2022, **61**, 10310–10320.

22 I. Choi, S. Chun and Y. K. Chung, *J. Org. Chem.*, 2017, **82**, 12771–12777.

23 M. Zhu, *Catal. Lett.*, 2014, **144**, 1568–1572.

24 Q. Lei, Y. Wei, D. Talwar, C. Wang, D. Xue and J. Xiao, *Chem. – Eur. J.*, 2013, **19**, 4021–4029.

25 C. T. Nandhu, T. Aneeja and G. Anilkumar, *J. Organomet. Chem.*, 2022, **122332**, 965–966.

26 C. Nogues and G. Argouarch, *ChemistrySelect*, 2020, **5**, 8319–8327.

27 Y. Yang, L. Zhou, X. Wang, L. Zhang, H. Cheng and F. Zhao, *Nano Res.*, 2023, **16**, 3719–3729.

28 J. S. Sapsford, D. J. Scott, N. J. Allcock, M. J. Fuchter, C. J. Tighe and A. E. Ashley, *Adv. Synth. Catal.*, 2018, **360**, 1066–1071.

29 J. Wang, C. Liu, L. Cao, Y. Xiong, J. Ye, Z. Liu and R. Cheng, *Mol. Catal.*, 2022, **527**, 112050.

30 A. Pagnoux-Ozherelyeva, N. Pannetier, M. D. Mbaye, S. Gaillard and J. L. Renaud, *Angew. Chem., Int. Ed.*, 2012, **51**, 4976–4980.

31 H. Hikawa, R. Ichinose, S. Kikkawa and I. Azumaya, *Green Chem.*, 2018, **20**, 1297–1305.

32 J. Liu, Y. Zhu, C. Wang, T. Singh, N. Wang, Q. Liu, Z. Cui and L. Ma, *Green Chem.*, 2020, **22**, 7387–7397.

33 L. Kathuria and A. G. Samuelson, *Eur. J. Inorg. Chem.*, 2020, **24**, 2372–2379.

34 L. Ouyang, Y. Xia, J. Liao and R. Luo, *Eur. J. Org. Chem.*, 2020, 6387–6391.

35 N. Wang, J. Liu, X. Li and L. Ma, *Catal. Commun.*, 2023, **175**, 106620.

36 M. K. Bhunia, D. Chandra, H. Abe, Y. Niwa and M. Hara, *ACS Appl. Mater. Interfaces*, 2022, **14**, 4144–4154.

37 T. Irrgang and R. Kempe, *Chem. Rev.*, 2020, **120**, 9583–9674.

38 B. Villa-Marcos, W. Tang, X. Wu and J. Xiao, *Org. Biomol. Chem.*, 2013, **11**, 6934–6939.

39 Z. J. Yao, P. Li, K. Li and W. Deng, *Appl. Organomet. Chem.*, 2018, **32**, e4239.

40 S. Ogo, K. Uehara, T. Abura and S. Fukuzumi, *J. Am. Chem. Soc.*, 2004, **126**, 3020–3021.

41 X. J. Yun, C. Ling, W. Deng, Z. J. Liu and Z. J. Yao, *Organometallics*, 2020, **39**, 3830–3838.

42 N. Kayacı, S. Dayan, N. Özdemir, O. Dayan and N. K. Özpozan, *Appl. Organomet. Chem.*, 2018, **32**, e4558.

43 M. Ruiz-Castañeda, M. C. Carrión, L. Santos, B. R. Manzano, G. Espino and F. A. Jalón, *ChemCatChem*, 2018, **10**, 5541–5550.

44 F. Christie, A. Zanotti-Gerosa and D. Grainger, *ChemCatChem*, 2018, **10**, 1012–1018.

45 S. Huang, X. Hong, H. Z. Cui, B. Zhan, Z. M. Li and X. F. Hou, *Organometallics*, 2020, **39**, 3514–3523.

46 S. A. Laneman and G. G. Stanley, *Homogenous Transitions Metal Catalysed Reaction Advances in Chemistry*, American Chemical Society, 1992, 230, 350–366.

47 L. Quebatte, E. Solari, R. Scopelliti and K. Severin, *Organometallics*, 2005, **24**, 1404–1406.

48 C. J. Mckenzi and R. Robson, *J. Chem. Soc., Chem. Commun.*, 1988, **7**, 112–114.

49 R. H. Lam, S. T. Keaveney, B. A. Messerle and I. Pernik, *ACS Catal.*, 2023, **13**, 1999–2010.

50 S. W. S. Choy, M. J. Page, M. Bhadbhade and B. A. Messerle, *Organometallics*, 2013, **32**, 4726–4729.

51 V. Diachenko, M. J. Page, M. R. D. Gatus, M. Bhadbhade and B. A. Messerle, *Organometallics*, 2015, **34**, 4543–4552.

52 H. Fujita, S. Takemoto and H. Matsuzaka, *ACS Catal.*, 2021, **11**, 7460–7466.

53 H. F. Yuen and T. J. Marks, *Organometallics*, 2009, **28**, 2423–2440.

54 K. Fukamizu, Y. Miyake and Y. Nishibayashi, *Angew. Chem., Int. Ed.*, 2009, **48**, 2534–2537.

55 S. C. Ammal, N. Yoshikai, Y. Inada, Y. Nishibayashi and E. Nakamura, *J. Am. Chem. Soc.*, 2005, **127**, 9428–9438.

56 Y. Nishibayashi, A. Shinoda, Y. Miyake, H. Matsuzawa and M. Sato, *Angew. Chem., Int. Ed.*, 2006, **45**, 4835–4839.

57 T. J. Steiman and C. Uyeda, *J. Am. Chem. Soc.*, 2015, **137**, 6104–6110.

58 D. Ghorai, L. H. Finger, G. Zanoni and L. Ackermann, *ACS Catal.*, 2018, **8**, 11657–11662.

59 H. Chai, T. Liu, D. Zheng and Z. Yu, *Organometallics*, 2017, **36**, 4268–4277.

60 T. Liu, H. Chai, L. Wang and Z. Yu, *Organometallics*, 2017, **36**, 2914–2921.

61 H. Chai, Q. Wang, T. Liu and Z. Yu, *Dalton Trans.*, 2016, **45**, 17843–17849.

62 P. Wehrmann and S. Mecking, *Organometallics*, 2008, **27**, 1399–1408.

63 R. Jangir, D. Kaleeswaran and R. Murugavel, *ChemistrySelect*, 2018, **3**, 8082–8094.

64 R. Jangir, M. Ansari, D. Kaleeswaran, G. Rajaraman, M. Palaniandavar and R. Murugavel, *ACS Catal.*, 2019, **9**, 10940–10950.

65 W. G. Jia, Z. B. Wang and X. T. Zhi, *Appl. Organomet. Chem.*, 2020, **34**, e5289.

66 R. Chatterjee, I. Bhattacharya, S. Roy, K. Purkait, T. S. Koley, A. Gupta and A. Mukherjee, *Inorg. Chem.*, 2021, **60**, 12172–12185.

67 X. Wu, X. Li, F. King and J. Xiao, *Angew. Chem., Int. Ed.*, 2005, **44**, 3407–3411.

68 C. Wang, C. Li, X. Wu, A. Pettman and J. Xiao, *Angew. Chem., Int. Ed.*, 2009, **48**, 6524–6528.

69 J. Niemeier, R. V. Engel and M. Rose, *Green Chem.*, 2017, **19**, 2839–2845.

70 Q. Zhang, S. S. Li, M. M. Zhu, Y. M. Liu, H. Y. He and Y. Cao, *Green Chem.*, 2016, **18**, 2507–2513.

71 J. T. Liu, S. Yang, W. Tang, Z. Yang and J. Xu, *Green Chem.*, 2018, **20**, 2118–2124.

72 D. Bhattacharyya, P. Adhikari, K. Deori and A. Das, *Catal. Sci. Technol.*, 2022, **12**, 5695–5702.

73 T. Abura, S. Ogo, Y. Watanabe and S. Fukuzumi, *J. Am. Chem. Soc.*, 2003, **125**, 4149–4154.

74 S. Patra, A. Kumar and S. K. Singh, *Inorg. Chem.*, 2022, **61**, 4618–4626.

75 J. B. Åberg, J. S. M. Samec and J. E. Bäckvall, *Chem. Commun.*, 2006, **26**, 2771–2773.

76 Y. Wei, D. Xue, Q. Lei, C. Wang and J. Xiao, *Green Chem.*, 2013, **15**, 629–634.

77 X. Wu, X. Li, A. Zanotti-Gerosa, A. Pettman, J. Liu, A. J. Mills and J. Xiao, *Chem. – Eur. J.*, 2008, **14**, 2209–2222.

78 C. Wang, C. Li, X. Wu, A. Pettman and J. Xiao, *Angew. Chem., Int. Ed.*, 2009, **48**, 6524–6528.

79 D. Talwar, X. Wu, O. Saidi, N. P. Salguero and J. Xiao, *Chem. – Eur. J.*, 2014, **20**, 12835–12842.

80 R. Ditchfield, W. J. Hehre and J. A. Pople, *J. Chem. Phys.*, 1971, **54**, 720–723.

81 P. J. Hay and W. R. Wadt, *J. Chem. Phys.*, 1985, **82**, 299–310.

82 A. Kumar, S. Ta, C. Nettem, J. M. Tanski, G. Rajaraman and P. Ghosh, *RSC Adv.*, 2022, **12**, 28961–28984.

83 F. Weigend and R. Ahlrichs, *Phys. Chem. Chem. Phys.*, 2005, **7**, 3297–3305.

84 J. Tomasi, B. Mennucci and R. Cammi, *Chem. Rev.*, 2005, **105**, 2999–3093.

85 E. D. Glendening, C. R. Landis and F. Weinhold, *J. Comput. Chem.*, 2013, **34**, 1429–1437.

86 Y. Guo, C. Riplinger, U. Becker, D. G. Liakos, Y. Minenkov, L. Cavallo and F. Neese, *J. Chem. Phys.*, 2018, **148**, 011101.

87 S. E. Neale, D. A. Pantazis and S. A. Macgregor, *Dalton Trans.*, 2020, **49**, 6478–6487.

88 F. Neese, *Wiley Interdiscip. Rev.: Comput. Mol. Sci.*, 2022, **2**, 73–78.

89 P. Paiva, M. J. Ramos and P. A. Fernandes, *J. Comput. Chem.*, 2020, **41**, 2459–2468.

90 F. Neese, *Wiley Interdiscip. Rev.: Comput. Mol. Sci.*, 2012, **2**, 73–78.

91 M. Broussard, B. Juma, S. G. Train, W. Peng, S. A. Laneman and G. G. Stanley, *Science*, 1993, **260**, 1784–1788.

92 M. J. Frisch, G. W. Trucks, H. B. Schlegel, G. E. Scuseria, M. A. Robb, J. R. Cheeseman, G. Scalmani, V. Barone, G. A. Petersson, H. Nakatsuji, X. Li, M. Caricato, A. V. Marenich, J. Bloino, B. G. Janesko, R. Gomperts, B. Mennucci, H. P. Hratchian, J. V. Ortiz, A. F. Izmaylov, J. L. Sonnenberg, D. Williams-Young, F. Ding, F. Lipparini, F. Egidi, J. Goings, B. Peng, A. Petrone, T. Henderson, D. Ranasinghe, V. G. Zakrzewski, J. Gao, N. Rega, G. Zheng, W. Liang, M. Hada, M. Ehara, K. Toyota, R. Fukuda, J. Hasegawa, M. Ishida, T. Nakajima, Y. Honda, O. Kitao, H. Nakai, T. Vreven, K. Throssell, J. A. Montgomery Jr., J. E. Peralta, F. Ogliaro, M. J. Bearpark, J. J. Heyd, E. N. Brothers, K. N. Kudin, V. N. Staroverov, T. A. Keith, R. Kobayashi, J. Normand, K. Raghavachari, A. P. Rendell, J. C. Burant, S. S. Iyengar, J. Tomasi, M. Cossi, J. M. Millam, M. Klene, C. Adamo, R. Cammi, J. W. Ochterski, R. L. Martin, K. Morokuma, O. Farkas, J. B. Foresman and D. J. Fox, *Gaussian 16, Revision C.01*, Gaussian, Inc., Wallingford CT, 2016.

93 *CrysAlisPRO*, Oxford Diffraction/Agilent Technol. UKLtd, Yarnton, Oxford, UK.

94 L. J. Farrugia, *J. Appl. Crystallogr.*, 2012, **45**, 849–854.

95 O. V. Dolomanov, L. J. Bourhis, R. J. Gildea, J. A. K. Howard and H. Puschmann, *J. Appl. Crystallogr.*, 2009, **42**, 339–341.

96 G. M. Sheldrick, *Acta Crystallogr., Sect. C: Struct. Chem.*, 2015, **71**, 3–8.